

## Chiral background for the two-pion exchange nuclear potential: A parametrized version

C.A. da Rocha\*

*Instituto de Física Teórica, Universidade Estadual Paulista, R. Pamplona, 145 - 01405-900 - São Paulo, SP, Brazil*

M.R. Robilotta†

*Instituto de Física, Universidade de São Paulo, C.P. 20516, 01452-990, São Paulo, SP, Brazil*

(Received 9 February 1995)

We argue that the minimal chiral background for the two-pion exchange nucleon-nucleon ( $NN$ ) interaction has nowadays a rather firm conceptual basis, which entitles it to become a standard ingredient of any modern potential. In order to facilitate applications, we present a parametrized version of a configuration space potential derived previously. We then use it to assess the phenomenological contents of some existing  $NN$  potentials.

PACS number(s): 21.30.+y, 12.39.Fe, 13.75.Cs

### I. INTRODUCTION

Nowadays there are several nucleon-nucleon potentials which reproduce experimental information with high precision [1–6]. In all of them, the long and medium range interactions are associated with the exchanges of one and two pions, whereas there is a wide variation in the way short distance effects are treated. This region is theoretically uncertain and good fits to the data usually require many free parameters. The availability of alternative models, although welcome, points out to the need of criteria for discriminating among the various potentials.

All potentials become progressively less reliable as one goes from large to short distances. The pionic tail of the interaction is quite well established and its only source of uncertainty is the value of the pion-nucleon coupling constant. It determines many observables of the deuteron and large angular momentum scattering [7–10]. As far as the next layer is concerned, one finds some consensus in the literature regarding the importance of delta intermediate states and pion-pion correlations. Nevertheless, the treatment of details of these interactions is not uniform, a fact reflected in the existence of different profile functions for a given component of the potential. It is in this framework that chiral symmetry may prove to be useful and provide guidelines for a proper assessment of the various existing potentials.

Chiral symmetry corresponds to the idea that strong interactions are approximately invariant under transfor-

mations of the group  $SU(2) \times SU(2)$ . This symmetry was developed in the 1960s, in the framework of hadron physics, but the reasons behind its successes became clear only after the formulation of QCD, the theory describing the basic interactions of quarks and gluons. In QCD the quark masses of the low-lying  $SU(2)$  multiplet are very small and the Lagrangian becomes chiral invariant when they are neglected. QCD predictions can be directly tested only at high energies, where perturbation makes sense. At low energies, on the other hand, its non-Abelian structure makes calculations very difficult, and one is forced to resort to effective hadronic theories. In order to remain as close as possible to the fundamental level, the hadronic Lagrangian must have the same symmetries as QCD, even the approximate ones, such as chiral symmetry.

One of the major successes of chiral symmetry at hadron level were the predictions made for low-energy  $\pi N$  scattering. Early chiral calculations of this process considered just minimal systems, containing only pions and nucleons [11,12]. Motivated by phenomenology, this model was extended and one has learned that chiral amplitudes at tree level, including nucleon and delta poles, rho exchanges and corrections associated with the  $\pi N$  sigma term do reproduce satisfactorily subthreshold and scattering data up to 300 MeV.

Chiral symmetry at the hadron level may be implemented by means of either linear or nonlinear Lagrangians. The fact that no serious candidate has been found for the  $\sigma$  meson favors the latter type of approach. There are two forms of nonlinear Lagrangians which are especially suited for the  $\pi N$  system. One of them is based on a pseudoscalar ( $PS$ )  $\pi N$  coupling supplemented by a scalar ( $S$ ) interaction, equivalent to the exchange of an infinitely massive  $\sigma$  meson, and denoted as  $PS + S$  scheme [Eq. (1)]. The other one employs a pseudovector ( $PV$ )  $\pi N$  interaction and a vector ( $V$ ) term, which could represent the exchange of an infinitely massive  $\rho$  meson, constituting the  $PV + V$  scheme [Eq. (2)]:

---

\*Present address: Department of Physics, FM-15, University of Washington, Seattle, WA 98195. Electronic address: carocha@nucthy.phys.washington.edu

†Electronic address: robilotta@if.usp.br

$$\mathcal{L}_{PS+S} = \cdots - g\bar{\psi} \left( \sqrt{f_\pi^2 - \phi^2} + i\boldsymbol{\tau} \cdot \boldsymbol{\phi} \gamma_5 \right) \psi \quad , \quad (1)$$

$$\begin{aligned} \mathcal{L}_{PV+V} = \cdots - \frac{1}{4f_\pi^2} \bar{\psi} \gamma^\mu \boldsymbol{\tau} \psi \cdot \boldsymbol{\phi} \times \partial_\mu \boldsymbol{\phi} \\ + \frac{g}{2m} \bar{\psi} \gamma^\mu \gamma_5 \boldsymbol{\tau} \psi \cdot \partial_\mu \boldsymbol{\phi} + \cdots \quad . \end{aligned} \quad (2)$$

Both approaches yield the very same amplitude for the  $\pi N$  scattering when the axial coupling constant  $g_A$  is equal to 1. The extension to the case  $g_A \neq 1$  can be done quite naturally in the  $PV + V$  approach, and a little less so in the  $PS + S$  case. The fact that physical results should be independent of the representation used to implement chiral symmetry was discussed in very general terms by Coleman, Wess, and Zumino [13]. In the case of  $\pi N$  interactions, this point was emphasized by Coon and Friar [14].

Chiral symmetry has very little to say about the one-pion exchange (OPE)  $NN$  potential since, in the  $PS + S$  approach, predictions for this component do not depend on the scalar interaction. Moreover,  $PS$  and  $PV$  couplings are equivalent. The intermediate range part of the interaction, on the other hand, is due to the exchange of two pions and closely related to an off-shell  $\pi N$  amplitude. Thus, as pointed out by Brown and Durso in 1971 [15], chiral symmetry is quite relevant in this region. In the first calculations of this component of the potential, chiral symmetry was included disguised in the form of soft-pion theorems [15,16]. Nowadays one has realized that the use of effective field theories makes the implementation of chiral symmetry into hadronic systems much easier.

In the early 1970s, approaches to the intermediate range  $NN$  interactions based on field theory disconsidered chiral symmetry. Nevertheless, they were very important in setting the method to tackle the problem. In 1970, Partovi and Lomon [17] performed a paradigmatic calculation based on Feynman diagrams, using just  $PS$  couplings without chiral counterterms. A little later, Partovi and Lomon [18] included the  $\sigma$  meson in their calculation, used chiral symmetry to determine the  $\sigma N$  coupling constant, but did not group diagrams into chiral families, producing a potential with an uneven number of loops. About 10 years later a rather comprehensive study was performed by Zuilhof and Tjon [19], who compared direct and crossed box diagrams obtained using both  $PS$  and  $PV$  couplings, without paying attention to chiral symmetry.

The first modern field theoretical calculation of the two-pion exchange nucleon-nucleon potential ( $\pi\pi$ E-NNP) with strong emphasis on chiral symmetry was produced by Ordóñez and van Kolck [20]. They applied the conceptual perturbative framework developed by Weinberg [21] in a systematic discussion of corrections to pure OPE interactions, associated with form factor effects, exchange of two pions, and three-body forces. The problem was formulated using  $PV$  coupling for the pion, and expressions were given in momentum space.

In 1992, Celenza, Pantziris, and Shakin [22] studied

the influence of chiral symmetry on the  $NN$  interaction at one-loop order. These authors considered both  $PS$  and  $PV$  pion-nucleon couplings in order to derive the qualitative features of the scalar-isoscalar component of the interaction. They employed tensor decompositions of diagrams in momentum space, and one of their main conclusions was that the irreducible isoscalar interaction is attractive.

In a series of independent works, other authors also addressed to the same problem, namely the determination of the role of chiral symmetry in the two-pion exchange  $NN$  interaction. A momentum space evaluation of the scalar-isoscalar component was produced by Birse [23], in the framework of the linear  $\sigma$  model. Friar and Coon [24] used a more general Lagrangian in order to obtain a momentum space potential for infinitely massive nucleons. Finally, in another calculation, we [25] used nonlinear Lagrangians based on covariant derivatives and obtained a nonrelativistic potential in coordinate space.

All these calculations [20,22–25] are based on chiral symmetry and should, in spite of technical differences, yield the same predictions for the two-pion exchange potential. However, inspection of the conclusions presented by the various authors shows that this is not the case. Discrepancies may be traced back to two different sources, namely the methods employed for regularizing divergent integrals and the procedures used to subtract the iterated OPEP. We consider here only the latter problem. It is well known that the meaning of an iteration is defined by the dynamical equation adopted in a given problem. Thus, the use of the relativistic Bethe-Salpeter equation [26] or the nonrelativistic reductions due to Brueckner and Watson [27] or Blankenbecler and Sugar [28] correspond to different forms for the potential. An explicit discussion of the nonrelativistic case can be found in Ref. [24], where it is shown that physics is independent of the particular approach employed.

Another important feature of the problem is that physical results in a consistent calculation should also not depend on the particular representation used in the implementation of chiral symmetry [13,14]. In our calculation [25], we have shown explicitly that both  $PS + S$  and  $PV + V$  Lagrangians correspond to the same nonrelativistic potential. Of course, there is no reason to expect that things would be different in the case of the Bethe-Salpeter equation. However, we believe that the explicit demonstration of this property in the relativistic framework may prove to be nontrivial. The basic idea of the Bethe-Salpeter equation is to decompose the full amplitude into two-particle propagators and irreducible kernels. In the  $PS + S$  case, this kind of decomposition poses no special problem. The  $PV + V$  case, on the other hand, is tricky, since its box diagram contains contributions in which the pole of the nucleon propagator is canceled and hence must be interpreted with great care. Cancellations of nucleon poles are, in fact, already present in the intermediate  $\pi N$  amplitude that determines the  $\pi\pi$ E-NNP [25,29]. Therefore, in the present state of the art, we believe that nonrelativistic potentials provide a much safer ground for the study of chiral symmetry.

The minimal chiral model for the  $\pi\pi$ E-NNP, involving

only pions and nucleons, has nowadays very solid conceptual foundations. It has attained the same status as the OPEP in the late 1960s and one may expect it to become a necessary ingredient of any modern  $NN$  potential. On the other hand, this minimal chiral model fails to reproduce experimental information in the case of the intermediate  $\pi N$  amplitude incorporated into the  $NN$  interaction. Thus, in the  $\pi\pi$ E-NNP, the minimal model corresponds to a contribution which is necessary, but not sufficient to describe reality. This requirement demands the inclusion of other fields and processes in the model. An extension, in the framework of chiral symmetry, has been recently considered by Ordóñez, Ray, and van Kolck [30], with promising results.

In all calculations of the chiral background to the  $\pi\pi$ E-NNP, results are given in form of cumbersome integrals, which must be evaluated numerically. In order to facilitate applications, in Sec. II of this work we present a parametrized version of our configuration space potential, valid up to 0.5 fm and completely free of cutoff parameters. The knowledge of the minimal chiral  $\pi\pi$ E-NNP may be used to assess the phenomenological content of a given potential. This information can be obtained by subtracting the OPEP from it and then comparing the remainder with the chiral two-pion exchange background. In Sec. III, we consider the de Tourreil-Rouben-Sprung

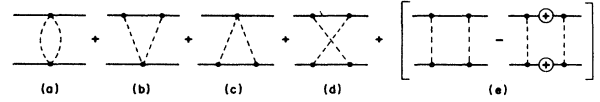


FIG. 1. Diagrams contributing to the minimal chiral background for the  $\pi\pi$ E-NNP. The vertices with one and two pions may be given by either  $PS$  and  $S$  or  $PV$  and  $V$  couplings [25]. The last diagram represents the subtraction of the iterated OPE from the reducible box diagram.

(dTRS) [2], Paris [3], and Argonne [5] potentials in order to produce an instance of this kind of study.

## II. PARAMETRIZATION

Our calculation of the  $\pi\pi$ E-NNP is based on the Blankenbecler-Sugar reduction of the Bethe-Salpeter equation. In the  $PS + S$  scheme, its dynamical content is associated with the five diagrams displayed in Fig. 1. Therefore we label the corresponding individual contributions by  $\emptyset$ ,  $\Delta$ ,  $\nabla$ , and  $\square$ , where the last one also includes the subtraction of the iterated OPEP. It has the general form<sup>1</sup>

$$\begin{aligned}
 V(r) = & \left[ \left( V_0^C + V_\Delta^C \right) + \hat{O}_{LS} \left( V_0^{LS} + V_\Delta^{LS} \right) \right] \\
 & + \left( 3 + 2\boldsymbol{\tau}^{(1)} \cdot \boldsymbol{\tau}^{(2)} \right) \left[ V_\infty^C + \hat{O}_{SS} V_\infty^{SS} + \hat{O}_{LS} V_\infty^{LS} + \hat{O}_T V_\infty^T \right] \\
 & + \left( 3 - 2\boldsymbol{\tau}^{(1)} \cdot \boldsymbol{\tau}^{(2)} \right) \left[ V_\square^C + \hat{O}_{SS} V_\square^{SS} + \hat{O}_{LS} V_\square^{LS} + \hat{O}_T V_\square^T \right], \quad (3)
 \end{aligned}$$

where the spin operators are given by  $\hat{O}_{SS} = \boldsymbol{\sigma}^{(1)} \cdot \boldsymbol{\sigma}^{(2)}$ ,  $\hat{O}_{LS} = \mathbf{L} \cdot \frac{1}{2} \{ \boldsymbol{\sigma}^{(1)} + \boldsymbol{\sigma}^{(2)} \}$ , and  $\hat{O}_T = 3\boldsymbol{\sigma}^{(1)} \cdot \hat{\mathbf{r}} \boldsymbol{\sigma}^{(2)} \cdot \hat{\mathbf{r}} - \boldsymbol{\sigma}^{(1)} \cdot \boldsymbol{\sigma}^{(2)}$ , whereas  $\boldsymbol{\sigma}^{(i)}$  and  $\boldsymbol{\tau}^{(i)}$  represent spin and isospin matrices for the nucleon ( $i$ ).

In the case of the bubble diagram, the leading contribution to the asymptotic potential can be calculated analytically, as shown in the Appendix. This result sets the pattern for the parametrization of the other components of the force.

Our numerical expressions represent the various components of the potential in MeV, and are given in terms of the adimensional variable  $x \equiv \mu r$ , where  $\mu$  is the pion mass. We keep the  $\pi N$  coupling constant  $g$  as a free parameter and adopt the values  $\mu = 137.29$  MeV and  $m = 938.92$  MeV for the pion and nucleon masses, respectively.

In general, the parametrized expressions reproduce quite well the numerical results of Ref. [25], except for

a few cases and regions where the discrepancies become of the order of 0.25%. Our results are listed below.

### A. Central potential

The profile function for the central potential has the following common multiplicative expression:

$$F_c(x) = \left( \frac{g\mu}{2m} \right)^4 \frac{e^{-2x}}{x^2 \sqrt{x}}. \quad (4)$$

The parametrization of each diagram gives

<sup>1</sup>See Eq. (59) of Ref. [25].

$$V_0^C(x) = F_c(x) \left\{ -275.364 - \frac{51.0923}{x} + \frac{6.540\,68}{x^2} - \frac{1.261\,90}{x^3} + \frac{0.130\,706}{x^4} \right\}, \quad (5)$$

$$V_\Delta^C(x) = F_c(x) \left\{ 343.558 - \frac{14.0446}{x} + (135.249 + 14.6514x + 6.43825x^2) e^{-0.397\,835x} \right\}, \quad (6)$$

$$V_\infty^C(x) = \frac{V_\Delta^C(x)}{12} + F_c(x) \left\{ -\frac{265.304}{\sqrt{x}} + \frac{518.531}{x} - \frac{577.210}{x\sqrt{x}} + \frac{378.004}{x^2} - \frac{133.374}{x^2\sqrt{x}} + \frac{19.5061}{x^3} \right\}, \quad (7)$$

$$V_\square^C(x) = F_c(x) \left\{ -25.9987 + \frac{8.337\,77}{x} - \frac{0.870\,724}{x^2} \right\} e^{-[0.101\,214x + 0.001\,236\,87x^2]}. \quad (8)$$

### B. Spin-spin potential

The multiplicative factor for the spin-spin potential is the same as that of the central potential, and receives contributions from the box and crossed diagrams only, which are given by

$$V_\infty^{SS}(x) = F_c(x) \left\{ 0.408\,084 + \frac{1.050\,42}{x} + \frac{0.421\,043}{x^2} - \frac{0.028\,430\,9}{x^3} - 0.215\,829 e^{-1.2344x} \right\}, \quad (9)$$

$$V_\square^{SS}(x) = F_c(x) \left\{ 0.399\,845 + \frac{1.071\,91}{x} + \frac{0.216\,302}{x^2} - \frac{0.030\,627\,1}{x^3} + 0.037\,133\,3 x e^{-0.168\,08x} \right\}. \quad (10)$$

### C. Spin-orbit potential

The spin-orbit multiplicative function is

$$F_{LS}(x) = \left( \frac{g\mu}{2m} \right)^4 \left( 1 + \frac{1}{2x} \right) \frac{e^{-2x}}{x^3\sqrt{x}}, \quad (11)$$

and individual contributions are

$$V_0^{LS}(x) = F_{LS}(x) \left\{ -5.887\,44 - \frac{5.510\,78}{x} + \frac{0.994\,157}{x^2} - \frac{0.217\,562}{x^3} + \frac{0.033\,606\,7}{x^4} - \frac{0.002\,446\,20}{x^5} \right\}, \quad (12)$$

$$V_\Delta^{LS}(x) = F_{LS}(x) \left\{ 7.345\,48 + \frac{2.152\,33}{x} - \frac{0.381\,025}{x^2} + (7.487\,98 - 0.448\,484x + 0.391\,431x^2) e^{-0.419\,984x} \right\}, \quad (13)$$

$$V_\infty^{LS}(x) = -\frac{V_\Delta^{LS}(x)}{4} + F_{LS}(x) \left\{ \frac{5.672\,35}{\sqrt{x}} - \frac{10.6417}{x} + \frac{14.7389}{x\sqrt{x}} - \frac{12.6506}{x^2} + \frac{6.273\,74}{x^2\sqrt{x}} - \frac{1.666\,37}{x^3} + \frac{0.184\,264}{x^3\sqrt{x}} \right\}, \quad (14)$$

$$V_\square^{LS}(x) = F_{LS}(x) \left\{ -1.195\,27 - \frac{1.580\,89}{x} + \frac{0.319\,790}{x^2} - \frac{0.019\,646\,1}{x^3} \right\} [1 - 0.016\,025\,9x]^{-1}. \quad (15)$$

### D. Tensor potential

The common factor for the tensor potential is

$$F_T(x) = \left( \frac{g\mu}{2m} \right)^4 \left( 1 + \frac{3}{2x} + \frac{3}{4x^2} \right) \frac{e^{-2x}}{x^2\sqrt{x}}. \quad (16)$$

It receives contributions from the box and crossed diagrams only, which have the form

$$V_\infty^T(x) = F_T(x) \left\{ -0.204\,041 - \frac{0.510\,720}{x} + \frac{0.059\,755\,6}{x^2} + (1.329\,32 - 0.939\,553x + 0.706\,050x^2) e^{-2.296\,86x} \right\}, \quad (17)$$

$$V_\square^T(x) = F_T(x) \left\{ -0.246\,349 - \frac{0.521\,123}{x} + \frac{0.352\,463}{x^2} - \frac{0.135\,028}{x^3} + \frac{0.030\,301\,2}{x^4} - \frac{0.002\,978\,40}{x^5} \right\}. \quad (18)$$

### III. PHENOMENOLOGY

As discussed in the Introduction, one may expect a realistic two-pion exchange nucleon-nucleon potential to be composed of a minimal chiral background supplemented by other terms determined by phenomenology. In this section we estimate crudely the relative weights of these two types of contributions, by comparing the parametrized expressions of the preceding section with three realistic potentials available in the literature, known as dTRS [2], Paris [3], and Argonne v14 [5].

In the minimal chiral potential the  $\pi N$  coupling constant may be kept as a free parameter, whereas in the realistic versions considered it assumes slightly different values. Therefore, in order to compare properly the various results, we subtract the OPEP contribution from each potential and then divide the remainder by the fourth power of the  $\pi N$  coupling constant used in it. We then consider, for various channels, the ratio of this quantity by that obtained from the parametrization of Sec. II with  $g = 1$ .

The ratios for the  $(T = 1, S = 0)$  central potential are displayed in Fig. 2. For distances greater than 7.5 fm, the ratio of the Argonne potential becomes a constant since, as the minimal chiral background, it behaves asymptotically as Yukawa functions with double pion mass. In the case of the dTRS potential, the ratio vanishes because it is relatively short ranged. The tail of the ratio of the Paris potential, on the other hand, is rather large and not stable up to 10 fm, probably due to the way it is parametrized.

The realistic potentials considered here reproduce well  $NN$  observables due to their behavior in the region below 2.5 fm. Inspecting Fig. 2 one notes that, in spite of important differences in this region, the three potentials display a sort of rough coherence. In all cases the fit of observables seem to require contributions with the

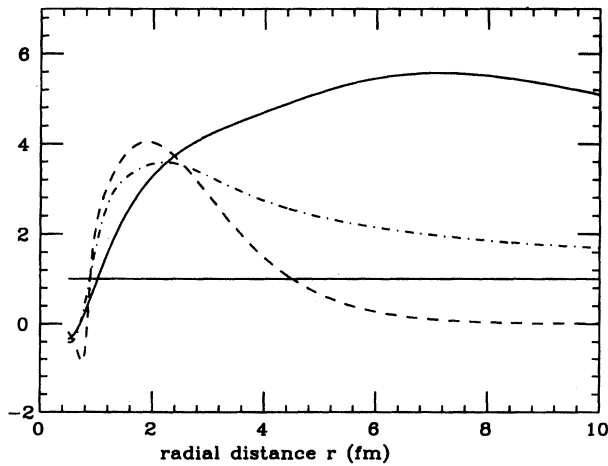


FIG. 2. Ratio between the non-OPEP part of the central  $(T = 1, S = 0)$  component of the dTRS [2] (dashed line), Argonne v14 [5] (dot-dashed line), and Paris [3] (continuous line) potentials divided by  $g^4$  and the minimal chiral background for the  $\pi\pi$ E-NNP.

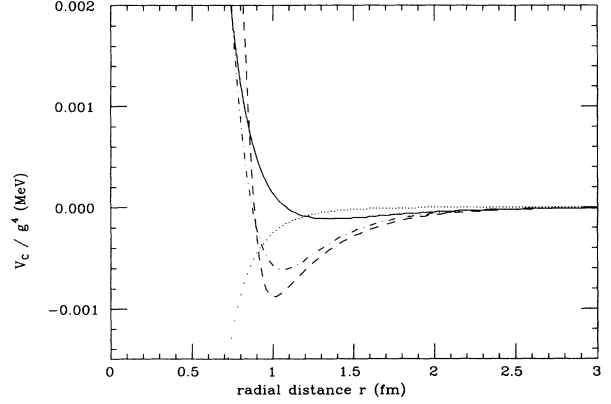


FIG. 3. Profile functions for the spin-isospin symmetric component of the dTRS [2] (dashed line), Argonne v14 [5] (dot-dashed line), Paris [3] (continuous line), and the chiral background (dotted line) potentials.

same sign and about four times bigger than the chiral background. The case of  $(T = 1, S = 1)$  central component is similar. The rough coherence among the realistic potentials is also present in the  $(T = 0, S = 0)$  and  $(T = 0, S = 1)$  central channels, but the ratios in the region between 1 and 2.5 fm are negative.

In Fig. 3 we show the profile function for  $V^C$ , the spin-isospin symmetric component of the central potential, which corresponds to the combination  $V^C = V_0^C + V_\Delta^C + 3V_\square^C + 3V_\infty^C$ , and is relevant for symmetric nuclear matter. The chiral background, in the physically relevant region, is much less attractive than the realistic forces.

In Fig. 4 we display the ratio of the  $(T = 0, S = 1)$  spin-orbit potentials. In this case there is no coherence among the realistic potentials, even regarding their signs. Both the tails and medium distance behaviors of the various ratios differ significantly from the background. The

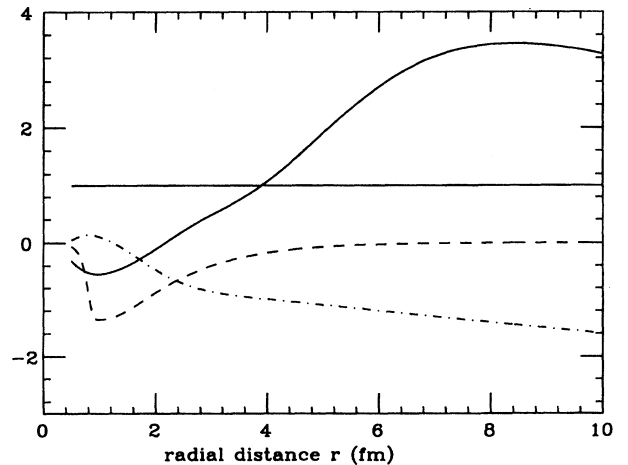


FIG. 4. Same as Fig. 2 for the  $(T = 0, S = 1)$  spin-orbit potential.

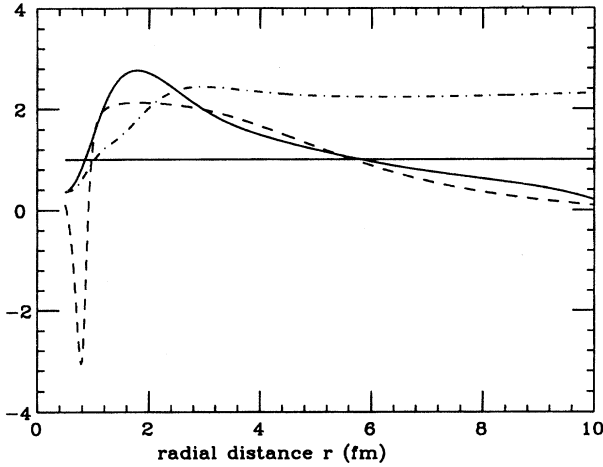


FIG. 5. Same as Fig. 2 for the  $(T = 1, S = 1)$  tensor potential.

$(T = 1, S = 1)$  component behaves similarly.

Finally, the ratios for the  $(T = 1, S = 1)$  tensor potential are given in Fig. 5, where it is possible to note that the realistic potentials are roughly coherent below 2.5 fm and about three times greater than the background. In the case of the  $(T = 0, S = 1)$  component, on the other hand, this ratio is about 5.

In summary, the crude comparisons made in this section allow one to conclude that the minimal chiral background for the two-pion exchange nuclear potential accounts for less than 25% of the values need in order to reproduce observations.

#### ACKNOWLEDGMENT

The work of one of us (C.A.R.) was supported by FAPESP, Brazilian Agency.

#### APPENDIX: ASYMPTOTIC BEHAVIOR OF THE BUBBLE DIAGRAM

The asymptotic behavior of the bubble diagram [Fig. 1(a)] can be calculated analytically. Its contribution to the potential is given by [25]

$$V_0 = i6 \frac{g^4}{4m^2} I^{(1)} I^{(2)} J_1, \quad (\text{A1})$$

where

$$J_1 = \int \frac{d^4 s}{(2\pi)^4} \frac{1}{\left[ \left( s - \frac{1}{2}\Delta \right)^2 - \mu^2 \right] \left[ \left( s + \frac{1}{2}\Delta \right)^2 - \mu^2 \right]}, \quad (\text{A2})$$

and  $\Delta$  is the momentum transferred. The operator  $I^{(1)} I^{(2)}$  has the following nonrelativistic spin structure:

$$I^{(1)} I^{(2)} = 1 - \frac{\hat{O}_{LS}}{2m^2}, \quad (\text{A3})$$

$\hat{O}_{LS}$  being the spin-orbit operator.

Using the Feynman parametrization and performing the integral in Eq. (A2), the function  $J_1$  may be written as

$$J_1(\Delta) = \frac{i}{(4\pi)^2} (\Lambda^2 - \mu^2) \int_0^1 d\alpha \int_0^{1-\alpha} d\beta \frac{4}{[(\alpha + \beta) - (\alpha - \beta)^2]} \frac{1}{\Delta^2 + M_1^2}, \quad (\text{A4})$$

where

$$M_1 = 2 \left[ \frac{(1 - \alpha - \beta)\Lambda^2 + (\alpha + \beta)\mu^2}{(\alpha + \beta) - (\alpha - \beta)^2} \right]^{1/2}, \quad (\text{A5})$$

$\Delta$  is the trimomentum exchanged in the interaction and  $\Lambda$  is a monopole cutoff regularizator. The corresponding expression in configuration space for  $J_1$  is given by

$$J_1(r) = i \frac{\Lambda^2 - \mu^2}{(4\pi)^3} 4 \int_0^1 d\alpha \int_0^{1-\alpha} d\beta \frac{1}{(\alpha + \beta) - (\alpha - \beta)^2} \frac{e^{-M_1 r}}{r}. \quad (\text{A6})$$

In the limit  $\Lambda \rightarrow \infty$ , the integrand is nonvanishing only in the neighborhood of the point  $(1 - \alpha - \beta) = 0$ . That means that, except in the term proportional to  $\Lambda^2$ , we may set  $\beta = 1 - \alpha$ . With this approximation, one has

$$J_1(r) = i 4 \frac{\Lambda^2 - \mu^2}{(4\pi)^3} \int_0^1 d\alpha \int_0^{1-\alpha} d\beta \frac{1}{D^2 r} e^{-2[(1-\alpha-\beta)\Lambda^2 + \mu^2]^{1/2}(r/D)}, \quad (\text{A7})$$

where

$$D^2 = 1 - (2\alpha - 1)^2. \quad (\text{A8})$$

Defining a new variable  $s$  by

$$s^2 = (1 - \alpha - \beta)\Lambda^2 + \mu^2, \quad (\text{A9})$$

one has

$$J_1(r) = i \frac{8}{(4\pi)^3} \int_0^1 d\alpha \frac{1}{D^2 r} \int_\mu^\infty ds s e^{-2sr/D}. \quad (\text{A10})$$

In deriving this result we used the fact that  $\Lambda$  is very large. Performing the integration and using the variable  $x \equiv \mu r$ , one obtains

$$J_1(r) = i \frac{4\mu^3}{(4\pi)^3} \int_0^1 d\alpha \left[ \frac{1}{D x^2} + \frac{1}{2x^3} \right] e^{-2x/D}. \quad (\text{A11})$$

For very large values of  $x$ , the main contribution to the integral comes from the region around  $\alpha = \frac{1}{2}$ , where  $D$  is maximum. In order to explore this property, we use the variable  $\theta = 2\sqrt{x}(\alpha - \frac{1}{2})$ , expand  $D$  around  $\theta = 0$  and write

$$J_1(x) = i \frac{2\mu^3}{(4\pi)^3} \frac{e^{-2x}}{x^2 \sqrt{x}} \int_{-\sqrt{x}}^{\sqrt{x}} d\theta \left[ 1 + \frac{1}{2x} \left( 1 + \theta^2 - \frac{3}{2}\theta^4 \right) \right] e^{-\theta^2}. \quad (\text{A12})$$

As  $x$  is large, the integral can be performed and one has

$$J_1(x) = i \frac{2\mu^3}{(4\pi)^3} \sqrt{\pi} \left( 1 + \frac{3}{16x} \right) \frac{e^{-2x}}{x^2 \sqrt{x}}. \quad (\text{A13})$$

The potentials are given by Eq. (A1):

$$V_0^C(x) = - \left( \frac{g\mu}{2m} \right)^4 \frac{e^{-2x}}{x^2 \sqrt{x}} \left[ \frac{48\sqrt{\pi}}{(4\pi)^3} \frac{m^2}{\mu} \right] \left( 1 + \frac{3}{16x} \right), \quad (\text{A14})$$

$$V_0^{LS}(x) = - \left( \frac{g\mu}{2m} \right)^4 \left( 1 + \frac{1}{2x} \right) \frac{e^{-2x}}{x^3 \sqrt{x}} \left[ \frac{48\sqrt{\pi}}{(4\pi)^3} \mu \right] \left( 1 + \frac{15}{16x} - \frac{9}{64x^2} \right). \quad (\text{A15})$$

The numerical value of the terms within square brackets is 275.299 for the central potential and 5.886 07 for the spin-orbit potential, and they should be compared with those given in Eqs. (5) and (12), respectively. This

result motivated the structure of the expressions used in the parametrization of the other components of the potential.

- 
- |  |  |
|--|--|
| <p>[1] R. de Tourreil and D.W.L. Sprung, Nucl. Phys. <b>A201</b>, 193 (1973).</p> <p>[2] R. de Tourreil, B. Rouben, and D.W.L. Sprung, Nucl. Phys. <b>A242</b>, 445 (1975).</p> <p>[3] M. Lacombe, B. Loiseau, J.M. Richard, R. Vinh Mau, J. Côté, P. Pires, and R. de Tourreil, Phys. Rev. C <b>21</b>, 861 (1980).</p> <p>[4] R. Machleidt, K. Holinde, and C. Elster, Phys. Rep. <b>149</b>, 1 (1987).</p> <p>[5] R.B. Wiringa, R.A. Smith, and T.L. Ainsworth, Phys. Rev. C <b>29</b>, 1207 (1984).</p> <p>[6] M.M. Nagels, T.A. Rijken, and J.J. de Swart, Phys. Rev. D <b>17</b>, 768 (1978).</p> <p>[7] T.E.O. Ericson and M. Rosa-Clot, Phys. Lett. <b>110B</b>, 193 (1982); Nucl. Phys. <b>A405</b>, 497 (1983).</p> <p>[8] J.L. Ballot, A. Eiró, and M.R. Robilotta, Phys. Rev. C <b>40</b>, 1459 (1989).</p> <p>[9] J.L. Ballot and M.R. Robilotta, Phys. Rev. C <b>45</b>, 986 (1992).</p> <p>[10] J.L. Ballot and M.R. Robilotta, J. Phys. G <b>20</b>, 1599 (1994).</p> <p>[11] S. Weinberg, Phys. Rev. Lett. <b>17</b>, 616 (1966).</p> | <p>[12] H.S. Mani, Y. Tomozawa, and Y.P. Yao, Phys. Rev. Lett. <b>18</b>, 1084 (1967).</p> <p>[13] S. Coleman, J. Wess, and B. Zumino, Phys. Rev. <b>177</b>, 2239 (1969); C.G. Callan, S. Coleman, J. Wess, and B. Zumino, Phys. Rev. <b>177</b>, 2247 (1969).</p> <p>[14] S.A. Coon and J.L. Friar, Phys. Rev. C <b>34</b>, 1060 (1986).</p> <p>[15] G.E. Brown and J.W. Durso, Phys. Lett. <b>35B</b>, 120 (1971).</p> <p>[16] M. Chemtob, J.W. Durso, and D.O. Riska, Nucl. Phys. <b>B38</b>, 141 (1972).</p> <p>[17] M.H. Partovi and E.L. Lomon, Phys. Rev. D <b>2</b>, 1999 (1970).</p> <p>[18] F. Partovi and E.L. Lomon, Phys. Rev. D <b>5</b>, 1192 (1972).</p> <p>[19] M.J. Zuilhof and J.A. Tjon, Phys. Rev. C <b>24</b>, 736 (1981); <b>26</b>, 1277 (1982).</p> <p>[20] C. Ordóñez and U. Van Kolk, Phys. Lett. B <b>291</b>, 459 (1992).</p> <p>[21] S. Weinberg, Phys. Lett. B <b>251</b>, 288 (1990); Nucl. Phys. <b>B363</b>, 3 (1991).</p> <p>[22] L.S. Celenza, A. Pantziris, and C.M. Shakin, Phys. Rev. C <b>46</b>, 2213 (1992).</p> <p>[23] M.C. Birse, Phys. Rev. C <b>49</b>, 2212 (1994).</p> |
|--|--|

- [24] J.L. Friar and S.A. Coon, Phys. Rev. C **49**, 1272 (1994).
- [25] C.A. da Rocha and M.R. Robilotta, Phys. Rev. C **49**, 1818 (1994).
- [26] E.E. Salpeter and H.A. Bethe, Phys. Rev. **84**, 1232 (1951).
- [27] K.A. Brueckner and K.M. Watson, Phys. Rev. **90**, 699 (1953); **92**, 1023 (1953).
- [28] R. Blankenbecler and R. Sugar, Phys. Rev. **142**, 1051 (1966).
- [29] J.C. Pupin, M.Sc. thesis, Instituto de Física Teórica, Universidade Estadual Paulista, São Paulo, 1994 (unpublished).
- [30] C. Ordóñez, L. Ray, and U. Van Kolck, Phys. Rev. Lett. **72**, 1982 (1994).